Batch Substitution Calibration of a Mems Microphone Array : Impact of Sensor Performance Dispersion on Directivity Estimation

Matthieu Hartenstein, Francois Ollivier, Fabrice Silva, Paul Luizard

BATCH SUBSTITUTION CALIBRATION OF A MEMS MICROPHONE ARRAY : IMPACT OF SENSOR PERFORMANCE DISPERSION ON DIRECTIVITY ESTIMATION

M. Hartenstein[1] *F. Ollivier*[1] *F. Silva*[2] *P. Luizard*[2,3,4]

[1] Institut Jean le Rond ∂'Alembert, Sorbonne Université, CNRS UMR 7190, Paris, France
[2] Aix Marseille Univ, CNRS, Centrale Marseille, LMA UMR 7031, Marseille, France
[3] Audio Communication Group, Technische Universität Berlin, Germany
[4] Univ. Grenoble Alpes, CNRS, Grenoble INP, GIPSA-lab, Grenoble, France

ABSTRACT

With their small size, embedded analog-to-digital converter, and low cost, MEMS microphones are good candidates when deploying arrays dedicated to 3 dimensional high resolution directivity measurements. Measuring the sensitivity and phase uncertainties across the sensors of such an array can help quantifying their impact on the performance of the array.

In this work, a batch substitution calibration procedure is proposed. It is used to calibrate an array compounded of 128 sub-arrays of 8 MEMS microphones. This allows to estimate the dispersion in sensitivity on the frequency range 100–2000 Hz, and higher bounds for the dispersions of the sensitivity and phase on the frequency range 100–5000 Hz. An analysis of the obtained sensitivity statistics at 1 kHz corroborates the results of a recent study. Eventually, Monte-Carlo simulations are run in order to assess the impact of the measured sensor sensitivity and phase dispersion levels when estimating sound source directivities.

Index Terms— MEMS microphone arrays, calibration, directivity estimation, uncertainty quantification

1. INTRODUCTION

The directivity function of a sound source describes the angular dependency of the acoustic pressure in the far-field. It is a useful quantity when analyzing the field radiated by complex sound sources [1], or when incorporating them in virtual audio environments [2]. However, obtaining 3 dimensional directivity data requires a high amount of acoustic pressure sensors. For such a purpose, MEMS microphones are, thanks to their small size, their low cost and their embedded analog-to-digital converters, a better choice than the costful and analog traditional condenser microphones. However, array measurements demand precision in the sensitivity and phase matching of the array components, and there is as yet no standard for calibrating MEMS.

This work is part of the *RayoVox* project funded by the French National Research Agency (ANR-21-CE42-0017, 2021-25).

Since 2014 [3], several studies have adapted the calibration procedures commonly used for the calibration of condenser microphones - namely reciprocity, comparison, and substitution - to the sensitivity calibration of a unique MEMS microphone [4, 5, 6]. MEMS microphone arrays can be composed of dozens, if not hundreds [7], of microphones. To ease and speed up the calibration process, batch calibration is thus needed. Havranek *et al* [3] design an omni-directional source for the purpose of planar array calibration. Their work unfortunately does not provide calibration data. Ahlefeldt *et al* [8] succeed in measuring sensitivity values on the frequency range 100 Hz to 10 kHz. However, they do not test the omni-directionality of their source. Refs. [9, 10] infer sensitivity values from diffuse-field measurements. However, the diffuse field hypothesis is difficult to reach in real-life experiments. Eventually, Wijnings *et al* [11] adapt the comparison calibration method to planar arrays of microphones. They succeed in obtaining both the sensitivity and phase deviations in a population of 8384 MEMS microphones at 1 kHz. In this work, we propose to apply the substitution calibration method to geometrically identical sub-components of a 1024 MEMS microphone array dedicated to directivity measurements. This method allows to obtain information on both sensitivity and phase dispersion on a broad frequency range.

The setup, signal processing framework, and results of the calibration experiment, are presented in Sec. 2. The impact of the obtained sensitivity and phase uncertainties on directivity estimation is evaluated in Sec. 3. Eventually, Sec. 4 draws conclusions on the proposed study.

2. CALIBRATION EXPERIMENT

2.1. Material and method

Experimental setup. The MEMS microphone array of interest is compounded of 128 sub-arrays. The sub-arrays are linear bars of 8 MEMS microphones (Invensense ICS 43434 [12]) as shown on Fig. 1. The bars were successively mounted on a dedicated support in the anechoic room at

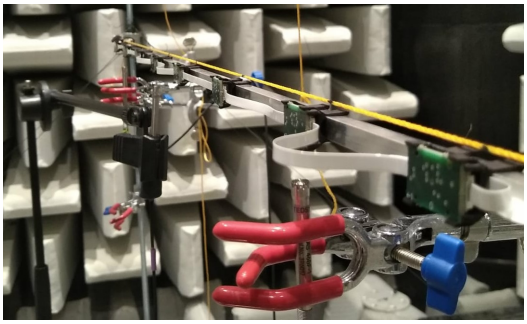

Fig. 1: A sub-array mounted on the calibration support.

LMA, the 8 sensors of each sub-array being placed at 8 positions, identical for all bars with a tolerance of about 1 mm.

The sub-arrays were then sequentially placed 2.5 m away from a broadband sound source (Genelec 8240A) driven by a Ferrofish A16 MK-II audio interface. Three additional quarter inch condenser microphones (GRAS 46 BF-1) were placed underneath. The acquisition system to which both the MEMS and the condenser microphones were connected is described in ref. [13]. A sampling frequency of 50 kHz was chosen for the acquisition. The same calibration signal - a synchronized exponential sweep [14] of 30 s seconds spanning the 50–20 000 Hz frequency range - was played for each bar. An analysis of the signals measured by the condenser microphones allowed to check the repeatability of the experiment on the frequency range 100–5000 Hz and the absence of source non-linearity.

Data processing. The post-processing used in the experiment is depicted in Fig. 2. The first step (*Frequency analysis* block) is to estimate the transfer functions $H^j_{s\to i}$ between the signal x_j sent to the sound source and the signal y^j_i acquired by the i^{th} microphone ($1 \leq i \leq 8$) of a given bar j ($1 \leq j \leq 128$). Power and cross spectral densities P_{x_j} and $P_{x_j y^j_i}$ are estimated from the Welch periodogram method [15] with a 2048 samples-long Hann window and 50 % overlap, resulting in a 25 Hz frequency resolution for the transfer function $H^j_{s\to i}$ defined as the ratio $P_{x_j y^j_i}/P_{x_j}$.

In a second step (block $\langle . \rangle_j$ in Fig. 2), the average transfer functions $H^{\text{avg}}_{s\to i}$ are computed for each of the 8 positions as

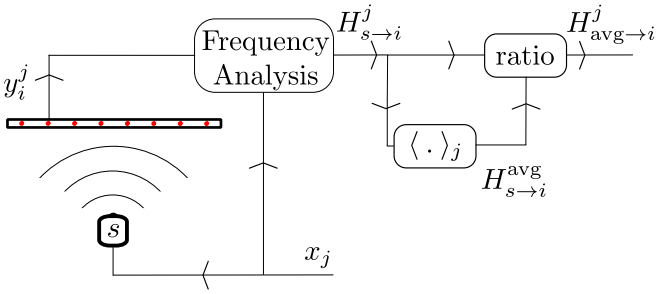

Fig. 2: Schematic of the data processing workflow.

the effective immitances obtained from averaging (over index j) the amplitudes (geometrical mean) and the phases (circular mean) obtained at positions i for all bars. These average transfer functions are to be interpreted as the nominal response of MEMS microphones at each given positions and their relevance will be discussed in the next section.

In the remainder of this section, we consider the relative response $H^j_{avg\to i}$ as the ratio between the individual transfer function $H^j_{s\to i}$ (estimated for microphone i of bar j) and the average transfer function $H^{\text{avg}}_{s\to i}$ (obtained from all measurements at position i). These relative responses are to be interpreted as individual deviation from the nomimal transfer function and should ideally not depend on the position i.

2.2. Results

Variability for a single microphone at a given position. Eight recordings have been made with bar $j = 0$ (mounting/unmounting the bar on the support). The estimated transfer functions $H^0_{s\to 0}$ obtained for the reference MEMS microphone ($(i, j) = (0, 0)$) evidence a standard deviation $\leq$ 0.05 dB below 1 kHz, $\leq$ 0.2 dB up to 5 kHz and $\leq$ 0.5 dB up to 10 kHz.

Relevance of the per-position averaged transfer functions. The same reference MEMS microphone ($(i, j) = (0, 0)$) has been moved to each of the 8 positions and the corresponding relative responses $H^{(0,0)}_{avg\to i}$ with respect to the per-position averaged transfer functions $H^{\text{avg}}_{s\to i}$ have been computed. The variability of these responses (given in terms of standard deviation of amplitude and phase over the 8 positions) is shown in Fig. 3 over the 100–5000 Hz frequency range.

The dispersion in sensitivity (solid line in top axis) slowly increases from ≈0.01 dB at 100 Hz to ≈0.1 dB at 2 kHz. These low dispersion values are a first clue that the sensitivity of an arbitrary MEMS at position i with respect to the average response at the same position does not depend on the measurement position. In the 2–5 kHz range, the sensitivity dispersion increases more steeply until 0.5 dB.

The phase dispersion (solid line in bottom axis) remains almost constant over the whole 100–5000 Hz frequency range, corresponding to an uncertainty of 0.5–1 mm in the location of the sensor. This dispersion in the estimated phase is higher than the phase dispersion of about 0.2 mm measured in [11]. These results are still consistent with the accuracy in the MEMS positioning (due to the mobility of the support) during the whole calibration process. The dispersion in sensor phase presented in the next section probably may thus overestimate the real phase dispersion in the sensor population. Despite this relatively high upper bound, the per-position average transfer functions appear to be robust references to achieve the calibration of the full set of MEMS microphones, with a lower variance than the responses of a single microphone acquired at each of the positions.

Variability of the relative transfer functions. Fig. 3 also

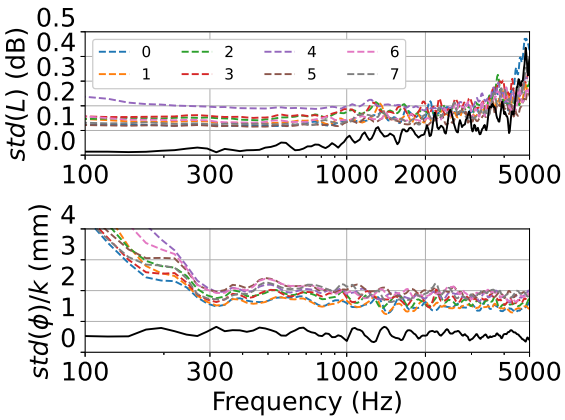

Fig. 3: Dashed color curves : standard deviation of the sensitivity (top) and phase (bottom) of the MEMS relatively to the average MEMS computed for the 8 population of 128 MEMS at the different calibration positions. One colour corresponds to one position. Continuous black curve : dispersion in the sensitivity and phase relative to the average MEMS of an arbitrary MEMS estimated from the 8 different measurement positions. The black curves are interpreted as sensitivity and phase estimation uncertainties. Phase dispersion is translated to distance by dividing by the acoustic wave number.

shows the standard deviation of the 128 estimated relative transfer functions $H^j_{avg\to i}$ for each of the 8 positions.

Firstly, the standard deviations of the sensitivities (dashed curves, top axis) show the same trend for all the positions ($\leq$0.15 dB up to 2 kHz), which means that the dispersion in sensitivity amongst the total of 1024 microphones tested is greater than the variability possibly introduced by the multiple-positions setup. Moreover, this can be read as an indication that the per-position estimated sensitivity distributions are representative of the global distribution.

From 2 to 5 kHz, the sensitivity dispersions become comparable to the variability related to the position. Thus, in this interval, it is only possible to infer higher bounds of sensitivity dispersion (up to 0.3–0.5 dB at 5 kHz).

As in Ref. [11], the distribution of the 1024 estimated sensitivities at 1 kHz were fitted as a Student's t-distribution with parameters $(\nu, \mu, \sigma) = (6.99, -0.01\,\text{dB}, 0.12\,\text{dB})$ (95 % confidence interval 0.36 dB) to be compared with the parameters obtained by Wijnings *et al* $(\nu, \mu, \sigma) = (7.56, 0.00\,\text{dB}, 0.16\,\text{dB})$ (95% confidence interval 0.39 dB, population of 8384 tested microphones).

Regarding the phase, the dispersion curves (dashed curves on the top plot of Figure3) are all equivalent to a 2 mm uncertainty in the sensor location from 300 Hz. At frequencies lower than 300 Hz, dividing by the acoustic wavenumber does not counter-balance the frequency dependency of the phase dispersion, which leads to higher equivalent distances of 3–4 mm. As highlighted in section 2.2, it is safer to read these phase dispersion levels as higher bounds of the phase dispersion. Note that when deploying large arrays of hundreds of microphones, the uncertainty in sensor location is higher than this level of dispersion, even when using automatic geometric calibration methods [16].

3. IMPACT OF DISPERSION OF SENSITIVITY AND PHASE ON DIRECTIVITY FACTOR ESTIMATION

Numerical simulations are performed to assess the robustness of a state-of-the-art directivity estimation method [17, 18] to variability in sensors performance as estimated in Sec. 2.

3.1. Numerical experiment

Directivity estimation method. The pressure field radiated by a source can be expanded onto a spherical wave basis as

$$p(r,\theta,\phi,k) = \sum_{n=0}^{+\infty}\sum_{m=-n}^{n} c_{mn}(k) h_n^{(2)}(kr) Y_n^m(\theta,\phi) \quad (1)$$

with (r,θ,ϕ) the spherical coordinates, k the wavenumber, $h_n^{(2)}$ the spherical Hankel functions of the second kind, Y_n^m the spherical harmonics, and $c_{mn}(k)$ the coefficients of the expansion. In the far-field, the Hankel functions behave as $j^{n+1}e^{-jkr}/r$ and equation (1) can be factored as [17]

$$p(r,\theta,\phi,k) \approx D_\infty(\theta,\phi)\frac{e^{-jkr}}{kr}. \quad (2)$$

Estimation of the far-field directivity function

$$D_\infty(\theta,\phi) = \sum_{n=0}^{\infty}\sum_{m=-n}^{n} c_{mn}(k) j^{n+1} Y_n^m(\theta,\phi). \quad (3)$$

of the source at any solid angle from pressure measurements is known as the directivity estimation problem. Truncating the outer sum in Eq. (1) to a finite maximal order N, the vector $\mathbf{c}$ of spherical harmonics coefficients can be estimated as the product of the regularized inverse of a sensing matrix $\mathbf{H}$ (with generic term $\mathbf{H}_{n(n+1)+m,q} = Y_n^m(\theta_q,\phi_q)h_n^{(2)}(kr)$. Hankel functions can exhibit significant amplitude variations from one order to another, hence the need for regularization) and a vector $\mathbf{p}$ of Q pressure measurements at given wavenumber k [17, 18]:

$$\hat{\mathbf{c}} = \left(\mathbf{H}^{\mathrm{H}}\mathbf{H} + \lambda\mathbf{I}\right)^{-1}\mathbf{H}^{\mathrm{H}}\mathbf{p}, \quad (4)$$

A continuous representation of the directivity function is then obtained from the truncated version of Eq. (3).

Generation of data. The radiation of a spherical cap source is considered here (rigid sphere of radius 8.5 cm with a vibrating aperture of radius 2 cm), as a first approximation of human voice radiation [19]. A surrounding spherical array (radius 1.5 m, same center as the source) supports 1024 microphones arranged following an equal-angle sensor distribution [20]. An axis-symmetrical Boundary Element model [21]

is used to synthetize both the measured fields at the positions of the sensors and a reference far-field directivity pattern D_∞^{ref} on an equal-angle reference spherical grid of $\approx$5000 points.

The far-field directivity function D_∞^{est} on the reference sphere is estimated using the directivity estimation method described above. The truncation order is chosen according to frequency using the far-field criterion defined in Ref. [18] with a maximal order $N = 12$. For the different experiments to be comparable, the regularization parameter λ used in Eq. (4) is set to 10^{-4}. The performance metric is the ratio of the L_2-norm of the error on the sphere to the L_2-norm of the solution

$$E = \frac{||\mathbf{\Omega}\left(\mathbf{D}_\infty^{\text{est}} - \mathbf{D}_\infty^{\text{ref}}\right)||_2}{||\mathbf{\Omega}\mathbf{D}_\infty^{\text{ref}}||_2}, \tag{5}$$

where $\mathbf{\Omega}$ accounts for integration on the reference grid.

Monte Carlo experiments. Monte-Carlo simulations (100 realizations) were run on the frequency range 100–5000 Hz to assess the impact of sensitivity and phase dispersion separately. In a first experiment, the sensitivities of all microphones is disturbed by the variable ΔL according to a centered normal distribution with standard deviation 0.3 dB (to be compared with the parameters of the Student t-distribution fit in Sec. 2). Due to the lack of information on the sensitivity distribution above 2 kHz, the Gaussian distribution was preferred here. In a second experiment, the phase of the sensors' transfer functions was disturbed by a quantity $\Delta\phi$ following a centered normal distribution with standard deviation corresponding to a position uncertainty of 2 mm. The standard deviations of ΔL and $\Delta\phi$ correspond to the maximal ones measured in the MEMS populations from Sec. 2.2 on the frequency range 100–5000 Hz. The pressure measurement of each sensor in Eq. (4) was noised by a scaling factor $10^{\Delta L/20}e^{j\Delta\phi}$ before being used in the directivity estimation method.

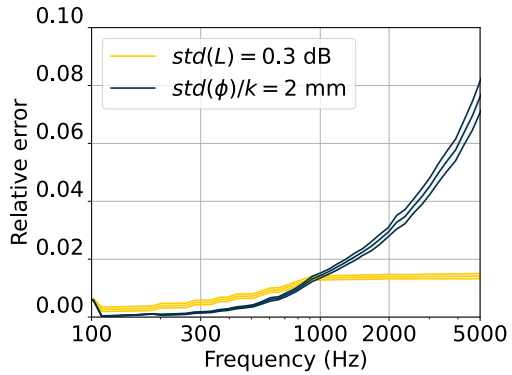

Fig. 4: Evolution with frequency of the mean (thick curves) and standard deviation (transparent zones delimited by thinner curves) of the performance metric E defined equation 5. Computed across 100 Monte-Carlo runs. The yellow curves are obtained with only sensitivity uncertainty, while the dark ones are obtained with only phase uncertainty.

3.2. Results

Fig. 4 shows the mean and standard deviation of the performance metric defined in Eq. (5) for the two Monte-Carlo experiments. Below 1 kHz, both conditions perform with no significant difference with averages and standard deviations of the performance metric slowly increasing to about respectively 1.4 % and 0.1 %. Above 1 kHz, the average and standard deviation of the error in presence of sensitivity uncertainty (yellow curves) stagnate at 1.4 % and 0.1 %. In the same frequency range, the mean error and standard deviation in presence of phase uncertainty increase, up to about 7 % and 0.5 %, respectively. Hence, both sources of uncertainty have the same impact up to 1 kHz, while the uncertainty in phase significantly prevails at higher frequencies.

4. CONCLUSION

A batch substitution calibration framework was proposed and applied to an array of 1024 MEMS microphones. It enabled the estimation of sensitivity dispersion across the array population over the frequency range 100–2000 Hz. To support this result, it was shown that the estimated distribution of sensitivity at 1 kHz are in line with the ones measured by Wijnings *et al* in Ref. [11]. From 2 to 5 kHz, the method gives a higher bound of 0.3 dB to the standard deviation for MEMS sensitivity. The results in terms of phase were more mitigated due to uncertainty in sensor location. Still, a higher bound equivalent to a 2 mm displacement was estimated for the phase standard deviation on the frequency range 300–5000 Hz. This phase uncertainty bound is slightly higher at lower frequencies.

Eventually, these higher bounds in sensitivity and phase uncertainties were used as inputs of Monte-Carlo experiments in order to assess the relative impact of sensitivity and phase dispersions on the estimation of directivity from measurements done with the MEMS microphone array. Both dispersions lead to similar errors and error uncertainty at lower frequencies, while phase dispersion is the main source of uncertainties at higher frequencies.

5. ACKNOWLEDGEMENTS

The authours would like to warmly thank Hélène Moingeon, Christian Ollivon, Marco Meinnel, Marc Pachebat and Cédric Pinhède for their help in preparing the experiment.

6. REFERENCES

[1] C. Pörschmann and J. M. Arend, "Analyzing the Directivity Patterns of Human Speakers," in *Proc. DAGA*, Hannover, Germany, 2020.

[2] S. Bilbao, J. Ahrens, and B. Hamilton, "Incorporating source directivity in wave-based virtual acoustics: Time-domain models and fitting to measured data," *The Journal of the Acoustical Society of America*, vol. 146, no. 4, pp. 2692–2703, Oct. 2019.

[3] Z. Havránek, P. Beneš, and S. Klusáček, "Free-field calibration of MEMS microphone array used for acoustic holograph," in *Proc. International Congress on Sound and Vibration*, Beijing, China, 2014.

[4] R. P. Wagner and S. E. Fick, "Pressure reciprocity calibration of a MEMS microphone," *The Journal of the Acoustical Society of America*, vol. 142, no. 3, pp. EL251–EL257, Sept. 2017.

[5] A. Prato, N. Montali, C. Guglielmone, and A. Schiavi, "Pressure calibration of a digital microelectromechanical system microphone by comparison," *The Journal of the Acoustical Society of America*, vol. 144, no. 4, pp. EL297–EL303, Oct. 2018.

[6] A. J. Zuckerwar, G. C. Herring, and B. R. Elbing, "Calibration of the pressure sensitivity of microphones by a free-field method at frequencies up to 80kHz," *The Journal of the Acoustical Society of America*, vol. 119, no. 1, pp. 320–329, Jan. 2006.

[7] H. Demontis, F. Ollivier, and J. Marchal, "Block-sparse approach for the identification of complex sound sources in a room," in *Proc. EAA Spatial Audio Sig. Proc. Symp.*, Paris, France, 2019.

[8] T. Ahlefeldt, S. Haxter, C. Spehr, D. Ernst, and T. Kleindienst, "Road to Acquisition: Preparing a MEMS Microphone Array for Measurement of Fuselage Surface Pressure Fluctuations," *Micromachines*, vol. 12, no. 8, pp. 961, Aug. 2021.

[9] M. Chan, C. Baker, D. Simmons, and M. Goldsmith, "Bulk calibration method of micro-electromechanical system (MEMS) microphones," *The Journal of the Acoustical Society of America*, vol. 150, no. 2, pp. 1402–1410, Aug. 2021.

[10] C. Vanwynsberghe, S. Bouley, and J. Antoni, "Gain and phase calibration of sensor arrays from ambient noise by cross-spectral measurements fitting," *The Journal of the Acoustical Society of America*, vol. 153, no. 2, pp. 1319–1330, Feb. 2023.

[11] P. W. Wijnings, S. Stuijk, R. Scholte, and H. Corporaal, "Characterization of Mems Microphone Sensitivity and Phase Distributions with Applications in Array Processing," in *Proc. Int. Conf. on Acoustics, Speech and Signal Processing (ICASSP) 2021*, Toronto, ON, Canada, 2021, pp. 4480–4484, IEEE.

[12] TDK Invensense, "ICS 43434 Datasheet," 2016.

[13] C. Vanwynsberghe, R. Marchiano, F. Ollivier, P. Challande, H. Moingeon, and J. Marchal, "Design and implementation of a multi-octave-band audio camera for realtime diagnosis," *Applied Acoustics*, vol. 89, pp. 281–287, Mar. 2015.

[14] A. Novak, P. Lotton, and L. Simon, "Synchronized Swept-Sine: Theory, Application, and Implementation," *Journal of the Audio Engineering Society*, vol. 63, no. 10, pp. 786–798, Nov. 2015.

[15] P. Welch, "The use of fast Fourier transform for the estimation of power spectra: A method based on time averaging over short, modified periodograms," *IEEE Transactions on Audio and Electroacoustics*, vol. 15, no. 2, pp. 70–73, June 1967.

[16] C. Vanwynsberghe, P. Challande, F. Ollivier, J. Marchal, and R. Marchiano, "Geometric calibration of very large microphone arrays in mismatched free field," *The Journal of the Acoustical Society of America*, vol. 145, no. 1, pp. 215–227, Jan. 2019.

[17] S. D. Bellows and T. W. Leishman, "Obtaining far-field spherical directivities of guitar amplifiers from arbitrarily shaped arrays using the Helmholtz equation least-squares method," in *Proc. Mtgs. Acoust.*, held online, Dec. 2020, vol. 42.

[18] M. Hartenstein, P. Luizard, H. Moingeon, C. Pinhède, M. Pachebat, C. Ollivon, F. Ollivier, and F. Silva, "A Method for Directivity Estimation with a High-Order Non-Spherical Microphone Array," in *Proc. Forum Acusticum*, Torino, Italy, 2023.

[19] J. L. Flanagan, "Analog Measurements of Sound Radiation from the Mouth," *The Journal of the Acoustical Society of America*, vol. 32, no. 12, pp. 8, 1960.

[20] B. Rafaely, *Fundamentals of Spherical Array Processing*, vol. 8 of *Springer Topics in Signal Processing*, Springer Berlin Heidelberg, 2015.

[21] V. C. Henríquez and P. M. Juhl, "OpenBEM - An open source Boundary Element Method software in Acoustics," in *Proc. Internoise*, Lisbon, Portugal, 2010, p. 10.